Available online at www.sciencedirect.com
ScienceDirect
Journal of Sound and Vibration 302 (2007) 50–66
JOURNAL OF SOUND AND VIBRATION
www.elsevier.com/locate/jsvi

Time reversal active sensing for health monitoring of a composite plate

Hyun Woo Park[a,1], Hoon Sohn[b,*], Kincho H. Law[c], Charles R. Farrar[d]

[a]Korea Bridge Design and Engineering Research Center, Seoul National University, Seoul, Korea
[b]Department of Civil and Environmental Engineering, Carnegie Mellon University, Pittsburgh 15213, USA
[c]Department of Civil and Environmental Engineering, Stanford University, CA 94305, USA
[d]Engineering Sciences and Applications Division, Los Alamos National Laboratory, NM 87545, USA

Received 7 May 2004; received in revised form 27 September 2006; accepted 31 October 2006
Available online 22 January 2007

Abstract

The applicability of a time reversal concept in modern acoustics to structural health monitoring was investigated. The time reversal method has been adapted to guided-wave propagation to improve the detectability of local defects in composite plate structures. Specifically, a wavelet-based signal processing technique has been developed to enhance the time reversibility of Lamb wave in thin composite plates. The validity of the proposed method is demonstrated through experimental studies in which input signals exerted at piezoelectric (PZT) patches on a quasi-isotropic composite plate are successfully reconstructed by using the time reversal method. The ultimate goal of this study is to develop a reference-free damage diagnosis technique based on the time reversal process so that defects can be identified without relying on any past baseline data.

1. Introduction

There has been a significant increase in the use of solid composites in load-carrying structural components, particularly in the aircraft and automobile industries. With the advances in sensor and hardware technologies that can generate and detect Lamb waves, many studies have been proposed to use Lamb waves for detecting defects in composite structures [1–4]. In particular, many researchers have recognized the potential use of piezoelectric (PZT) actuators/sensors for Lamb-wave-based structural health monitoring [2,4,5].

Lamb waves are mechanical waves whose wavelength is in the same order of magnitude as the thickness of the plate. The analysis and interpretation of Lamb waves can be complicated due to their dispersive and multimodal natures. The various frequency components of Lamb waves travel at different speeds and the shapes of wave packets change as they propagate through a solid medium. Multiple symmetric and anti-symmetric wave modes are generated as the driving frequency for wave generation increases.

*Corresponding author. Tel.: +1 412 268 2077; fax: +1 412 268 7813.
E-mail address: hsohn@cmu.edu (H. Sohn).
[1]Formerly appointed as a postdoctoral scholar during 2003–2004 in the Department of Civil and Environmental Engineering at Stanford University, CA 94305, USA.

0022-460X/$ - see front matter © 2006 Elsevier Ltd. All rights reserved.
doi:10.1016/j.jsv.2006.10.044

Recently, attention has been paid to the time reversal method developed in modern acoustics to compensate the dispersion of Lamb waves and to improve the signal-to-noise ratio of propagating waves [6–9]. For instance, a pulse-echo time reversal method, that is, the time reversal method working in pulse-echo mode has been employed to identify the location and size of defects in a plate [7–9]. However, if there exist multiple defects in a plate, this iterative pulse-echo process tends to detect only the most distinct defect, requiring more sophisticated techniques to detect multiple defects. Furthermore, the pulse-echo process seems impractical for structural health monitoring applications, because a dense array of sensors is required to cover the entire boundary of the plate being investigated.

In the time reversal method, an input signal can be reconstructed at an excitation point (point A) if an output signal recorded at another point (point B) is reemitted to the original source point (point A) after being reversed in a time domain as illustrated in Fig. 1. This time reversibility (TR) of waves is based on the spatial reciprocity and time reversal invariance of linear wave equations [10,11]. The specific goal of the research described in this paper is to reconstruct the known excitation signal at the original input location through the time reversal process of Lamb waves. In this study, an enhanced time reversal method is proposed so that the

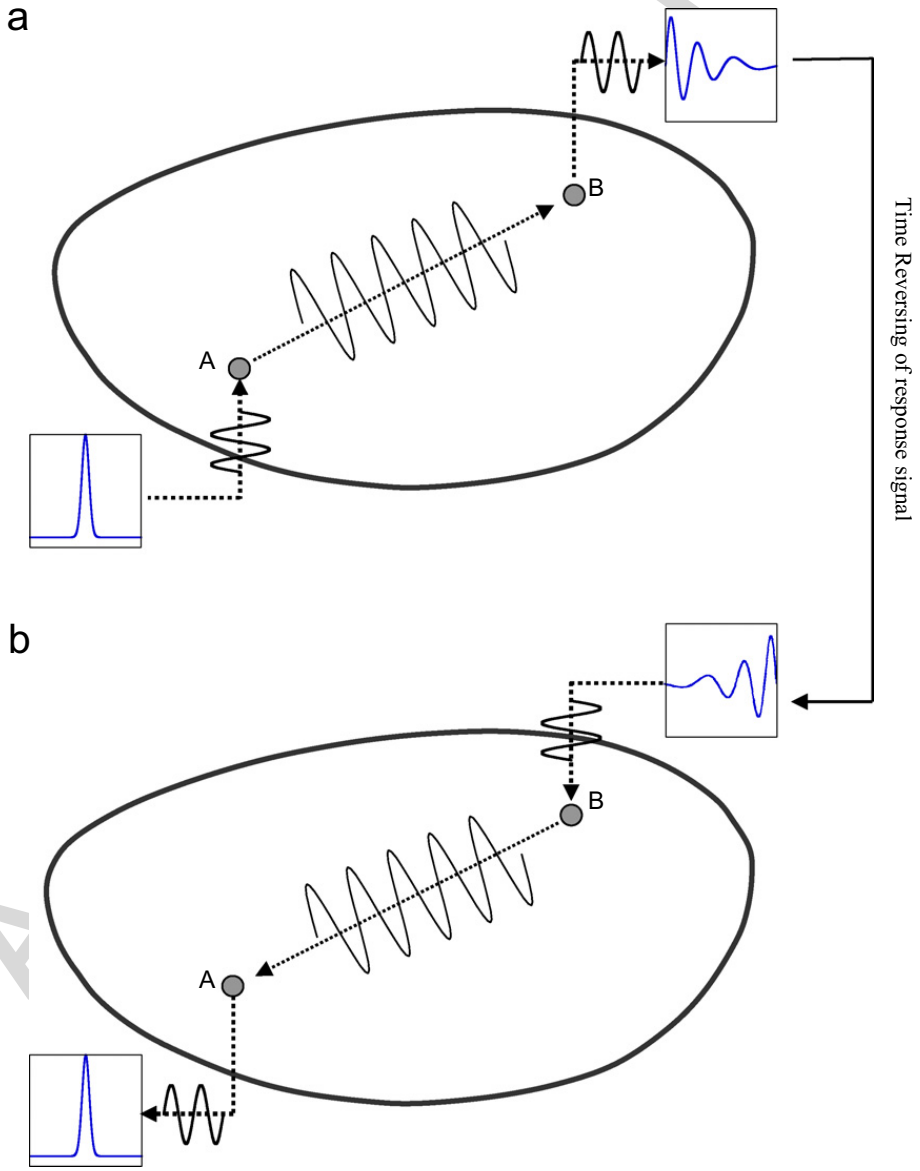

Fig. 1. Time reversal concept: (a) exerting input waves and (b) reemitting response waves being reversed with time.

reconstruction of the input signal can be achieved for Lamb wave propagation. The ultimate goal is to use this TR of Lamb waves for damage diagnosis.

Although the application of the time reversal concept to Lamb waves is not a new idea [8,12], the full reconstruction of the input signal has not been attempted before for Lamb waves. To achieve this goal, a specific narrowband input waveform and a wavelet-based signal filtering technique are employed to enhance the TR of Lamb waves. The complete reconstruction of the input signal cannot be achieved when a broad-band excitation is employed for Lamb wave propagations. Due to the frequency dependence of the time reversal process of Lamb waves, different frequency components of the broad-band excitation are scaled differently during the time reversal process and the original input signal cannot be fully restored. This is the primary reason for using a narrowband excitation. Once this TR is enforced for Lamb waves, our vision is to detect certain types of defects by examining the deviation of the reconstructed signal from the original input signal without relying on any past baseline data.

Often damage detection problems are cast in the context of statistical pattern comparison in which a damage state of the system is inferred by comparing test data with baseline data. However, the dependency of damage diagnosis on the prior baseline data makes the field deployment of current damage detection technologies extremely difficult. For instance, subtle signal changes due to damage could often be masked by larger operational and environmental variations of the in-service structure. In addition, the test data corresponding to a case where there may be damage are often collected long after the baseline data were recorded when the structure was in pristine condition. Therefore, the development of this baseline-free damage diagnosis technique can address the issue of minimizing false-positive indications of damage due to varying operational and environmental conditions. The validity of the proposed method is demonstrated through experimental studies of a quasi-isotropic composite plate, in which input signals exerted at PZT patches are successfully reconstructed during the time reversal process. Its application to actual damage diagnosis is reported elsewhere.

This paper is organized as follows: first, an analysis of Lamb waves using the Mindlin plate theory is described in Section 2; in Section 3, the TR of Lamb waves is investigated by introducing a time reversal operator in a frequency domain; the wavelet-based signal processing techniques to enhance the TR of Lamb waves are discussed in Section 4; numerical examples and experimental investigations are presented in Section 5 to demonstrate the validity of the enhanced time reversal method; and finally, this paper is concluded in Section 6 with a brief summary and discussions.

2. Lamb waves in a composite plate

Lamb waves usually occur on waveguides such as bars, plates and shells. Unlike body waves, the propagation of Lamb waves is complicated due to two unique features: dispersion and multimode characteristics [13]. Theoretically, these two features can be investigated by solving the Rayleigh–Lamb equations defined for the symmetrical and anti-symmetrical modes on an infinite plate with a thickness $2h$:

$$(k^2+s^2)^2\cosh(qh)\sinh(sh)-4k^2qs\sinh(qh)\cosh(sh)=0, \tag{1a}$$

$$(k^2+s^2)^2\sinh(qh)\cosh(sh)-4k^2qs\cosh(qh)\sinh(sh)=0, \tag{1b}$$

where $q^2=k^2-k_l^2$ and $s^2=k^2-k_t^2$. Furthermore, k denotes a wave number, and k_l and k_t are the wave numbers for the longitudinal and shear modes, respectively. It should be noted that there exist multiple wave modes that satisfy Eq. (1a). The dispersion curve can be expressed in terms of the product of the excitation frequency and the plate thickness versus the group velocity C_g, which is defined as

$$C_g=\frac{\mathrm{d}\omega}{\mathrm{d}k}, \tag{2}$$

where ω denotes an angular frequency. For a uniform plate with constant thickness, the dispersion curve can be represented as a function of the frequency as shown in Fig. 2.

As shown in Fig. 2, multiple Lamb wave modes are created as the excitation frequency increases. The dispersive nature of waves causes the different frequency components of Lamb waves to travel at different

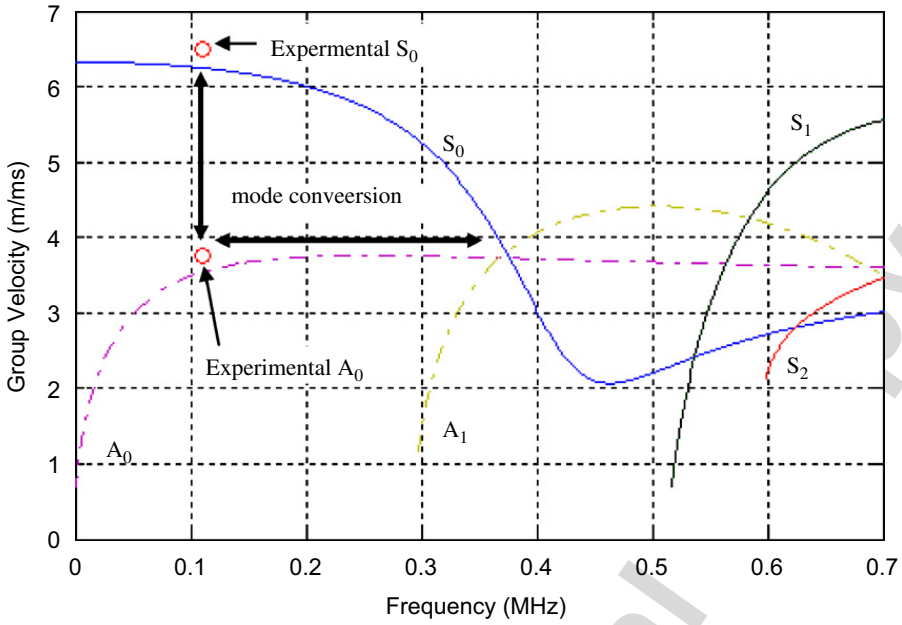

Fig. 2. A dispersion curve for an idealized isotropic composite plate (the abscissa is presented in terms of the frequency with the constant plate thickness (0.64 cm) rather than the frequency–thickness product). '—' S_0 mode, '……' A_0 mode, '-·-' S_1 mode, '---' A_1 mode, '–· ·' S_2 mode, '●' experimental S_0 mode at 110 kHz, '◆' experimental A_0 mode at 110 kHz and '↔' mode conversion.

speeds and thus the shape of the wave packet changes as it propagates through a solid medium. Due to the dispersive and multimodal characteristics of Lamb waves, it is difficult to analyze the wave signals and to identify existence of damage. Therefore, often a narrowband input signal is generated and its exciting frequency is selected so that (1) only two fundamental modes, namely the first symmetrical S_0 mode and anti-symmetrical A_0 mode, are generated and (2) the velocity dispersion of these modes can be reduced. For example, from Fig. 2 it can be seen that a 110 kHz narrowband excitation would satisfy these requirements; it was used in the numerical and experimental examples presented later in this paper. For the given layout of the PZT actuators and sensors discussed in Section 5, the magnitude of the S_0 mode is rather small and negligible compared to that of the A_0 mode [2]. Therefore, the discussion below focuses on the A_0 mode only.

The exact solution of the Lamb wave propagation problem can be quite complicated. Here, approximate wave equations based on the Mindlin plate theory are employed to predict the wave propagation of the A_0 mode and to validate the experimental results [5]. In the Mindlin plate theory, the Navier–Cauchy equations of three-dimensional elasticity for a plate are idealized and simplified in terms of a deflection and two rotations along the neutral plane of the plate. Particularly, the Mindlin plate theory can be used for predicting the A_0 mode propagating on a quasi-isotropic composite plate if the effective transverse-shear modulus is determined appropriately [14].

When an arbitrary PZT patch (A) is used as an actuator and another distinct PZT patch (B) is used as a sensor, as shown in Fig. 3, the response voltage at the sensing PZT patch B can be represented as follows:

$$V_B(r,\omega) = K_s(\omega)\hat{E}_B(r,\omega), \tag{3}$$

where r, $\hat{V}_B$, K_s and $\hat{E}_B$ are the wave propagation distance from the center of the actuating PZT patch to the sensing PZT patch, the response voltage at the sensing patch B, the mechanical-electro-efficiency constant and the surface strain at the center of patch B with respect to the angular frequency ω, respectively.

The surface strain at patch B can be rewritten as follows:

$$\hat{E}_B(r,\omega) = \hat{I}_A(\omega)K_a(\omega)G(r,\omega), \tag{4}$$

where $\hat{I}_A$, K_a and G are the input voltage at patch B, the counterpart of the mechanical-electro-efficiency K_s in Eq. (3) and the *frequency response function* of patch B as a result of the input at patch A, respectively. Specifically, the *frequency response function* G is obtained by applying appropriate transformation techniques

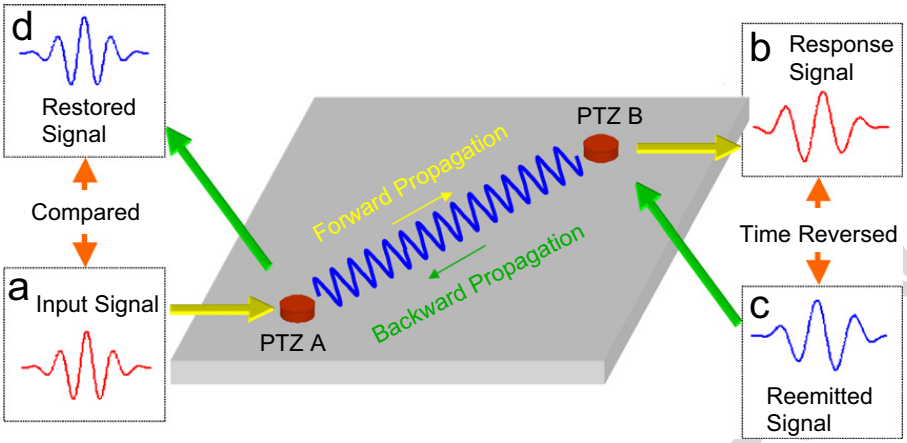

Fig. 3. Generation and sensing of Lamb waves on a plate by using PZT patches.

in the spatial domain and the time domain to the wave equations based on the Mindlin plate theory [14]:

$$G(r,\omega) = -\frac{i\pi h^2}{2D}\frac{\gamma_1 k_1^3 a J_1(k_1 a) H_0^{(1)}(k_1 r)}{k_1^2 - k_2^2}, \tag{5}$$

where D, γ_1, a, $J_1(\cdot)$ and $H_0^{(1)}(\cdot)$ are the flexural stiffness of the plate, the ratio of the dilatational wave to the vertical wave motion of the plate at the wave number k_1, the radius of PZT patch A, the first-order Bessel function and the zeroth-order Hankel function of first kind, respectively. The wave numbers, k_1 and k_2 determined at the A_0 mode and the second flexural A_1 mode of the plate, respectively. The propagation of the A_0 mode can be numerically simulated by using Eq. (4). This numerical prediction will be compared with experimental results in a subsequent session.

Note that the Bessel function in Eq. (5) is not only a function of the PZT radius (a) but also affected by the wave number (k_l). Because the wave number is a function of the density, flexural stiffness and thickness of the plate, the wave propagation characteristics described in Eq. (5) depend on the fundamental properties of the plate.

3. Time reversal lamb waves in a composite plate

The origin of the time reversal method traces back to time reversal acoustics [9,11]. In time reversal acoustics, an input body wave can be exactly reconstructed at the source location if a response signal measured at a distinct location is time-reversed (literally the time point at the end of the response signal becomes the starting time point) and reemitted to the original excitation location. This phenomenon is referred to as TR of body waves and has been used in applications such as lithotripsy, ultrasonic brain surgery, non-destructive evaluation and acoustic communications [9].

While the time reversal method for non-dispersive body waves in fluids has been well-established, the study of the time reversal method for Lamb waves on plates is still relatively new. Because of the dispersion characteristic of Lamb waves, wave packets traveling at higher speeds arrive at a sensing point earlier than those traveling at lower speeds. However, during the time reverse process at the sensing location, the wave packets, which travel at slower speeds and arrive at the sensing point later, are reemitted to the original source location first. Therefore, all wave packets traveling at different speeds concurrently converge at the source point during the time reversal process, compensating for the dispersion. The application of the time reversal method to Lamb wave propagation can compensate the dispersion effect, which has limited the use of Lamb waves for damage detection applications [7,8]. The effect of dispersion on the time reversal analysis of Lamb waves in a homogeneous plate was first studied by Wang et al. [5] by introducing the time reversal operator into the Lamb wave equation based on Mindlin plate theory.

While a number of experimental results have shown that the dispersion of Lamb waves is well compensated through the time reversal process, the TR of Lamb waves has not been fully investigated unlike that of body

waves. This study employs a narrowband excitation signal and a wavelet-based signal processing technique, not only to reduce the frequency dependence of the time reversal process to an acceptable tolerance level, but also to achieve a full reconstruction of the input signal.

3.1. TR of Lamb waves in a thin plate

With reference to Fig. 3, once a response signal, due to the original input signal at PZT patch A, is measured at PZT patch B, the reconstructed input signal at PZT patch A can be obtained by reemitting the time-reversed response signal at PZT patch B. Note that the time reversal operation of a signal in the time domain is equivalent to taking the complex conjugate of the Fourier Transform of the signal in the frequency domain. Therefore, the time reverse operation on the response signal at PZT patch B is equivalent to taking the complex conjugate of Eq. (3) in the frequency domain:

$$\hat{V}_B(r,\omega) = K_s^*(\omega)\hat{E}_B^*(r,\omega), \tag{6}$$

where a superscript * denotes a complex conjugate.

The reconstructed signal at PZT patch A from the reemitted signal at PZT patch B can be represented in a similar fashion as Eq. (3)

$$\hat{V}_A(r,\omega) = K_s(\omega)\hat{E}_A(r,\omega), \tag{7}$$

where

$$\hat{E}_A(r,\omega) = \hat{V}_B^*(r,\omega)K_a(\omega)G(r,\omega). \tag{8}$$

By using Eqs. (4), (6), (17) and (8), the Fourier transform of the reconstructed signal can be rewritten as

$$\hat{V}_A(r,\omega) = \hat{I}_A^*(\omega)K_a^*(\omega)K_s^*(\omega)K_a(\omega)K_s(\omega)G(r,\omega)G^*(r,\omega). \tag{9}$$

Performing an inverse Fourier transform, the reconstructed input signal $\tilde{V}_A$ at PZT patch A is

$$\tilde{V}_A(t) = \frac{1}{2\pi}\int_{-\infty}^{\infty} \hat{I}_A^*(\omega)K_{as}^*(\omega)K_{as}(\omega)G^*(r,\omega)G(r,\omega)\mathrm{e}^{\mathrm{i}\omega(T-t)}\,\mathrm{d}\omega, \tag{10}$$

where K_{as} denotes the product between K_a and K_s and T represents the total time period for the signal. If the TR of waves was satisfied, the reconstructed signal $\hat{V}_A(t)$ in Eq. (10) would be identical to the time-reversed original signal $I_A(T-t)$. To directly compare with the original input signal $I_A(t)$ at PZT patch A, Eq. (10) should be time reversed, thus:

$$\tilde{V}_A(T-t) = \frac{1}{2\pi}\int_{-\infty}^{\infty} \hat{I}_A(\omega)K_{TR}(\omega)G_{TR}(r,\omega)\mathrm{e}^{-\mathrm{i}\omega t}\,\mathrm{d}\omega, \tag{11}$$

where

$$K_{TR}(\omega) = K_{as}(\omega)K_{as}^*(\omega), \quad G_{TR}(\omega) = G(r,\omega)G^*(r,\omega). \tag{12}$$

Here, K_{TR} is a constant determined by the electro-mechanical efficiency of the PZT patch, and G_{TR} is referred to as a time reversal operator of Lamb waves in the Mindlin plate theory. In Eq. (11), the TR is achieved only if K_{TR} and G_{TR} are independent of the angular frequency ω. However, because the impulse response function $G(r,\omega)$ of a plate structure is frequency dependent and the time reversal operator is defined as $G(r,\omega)\ G^*(r,\omega)$, the time reversal operator G_{TR} varies with respect to the frequency. This indicates that the wave components at different frequency values are non-uniformly scaled as shown in Fig. 4 due to the fundamental properties of the plate. Therefore, the original input signal cannot be properly reconstructed if a broad-band input signal is used.

To alleviate this problem, a narrowband excitation signal is used with a multiresolution signal analysis technique so that the time reversal method yields a reconstructed signal sufficiently close to the emitted signal. Note that when a single frequency input is used, the frequency dependence shown in Eq. (12) disappears, allowing for proper reconstruction of the original input signal. In Section 4, the time reversal method is further improved by incorporating a well-designed narrowband input waveform and using a wavelet transform.

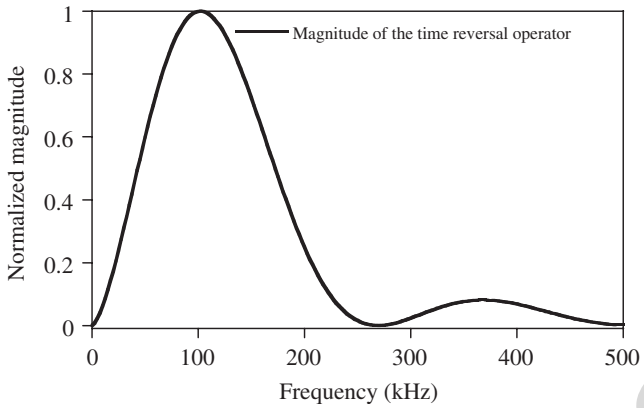

Fig. 4. Normalized time reversal operator of the A_0 mode.

To justify the use of a narrowband excitation for the time reversal process, a numerical example of the time reversal process is provided here. In particular, a broad-band (a Gaussian pulse as shown in Fig. 5(a)) and a narrowband 100 kHz tone burst, as shown in Fig. 5(d), are used as input signals in a numerical simulation of the time reversal process. The specifications for the composite plate and the PZT pair used in this numerical simulation are identical to those used in Section 5. The distance between the PZT pair is assumed to be long enough (5*m*) so that the velocity dispersion of Lamb waves can be observed at the response PZT, see Figs. 5(b) and (e). When the response signals are reversed in time and reemitted to the input PZT, the velocity dispersion of Lamb waves is compensated as shown in Figs. 5(c) and (f). However, the shape of the original pulse is not fully recovered when the Gaussian input is used as illustrated in Fig. 5(c). This is because the various frequency components of the Gaussian input are differently scaled and superimposed during the time reversal process as indicated in Fig. 4. On the other hand, as shown in Fig. 5(f), the shape of reconstructed tone burst waveform is practically identical to that of the original input tone burst because the amplification of the time reversal operator is almost uniform in this limited frequency band.

3.2. *Application of time reversal Lamb waves to delamination detection in a composite plate*

Intact composites possess atomic linear elasticity as water and copper do. The atomic elastic material is well described by the classical linear elastic constitutive law and linear wave propagation equations. However, it should be noted that the atomic elastic materials demonstrate nonlinear mesoscopic elasticity that appears to be much like that in rock or concrete if they have been damaged. Nonlinear mesoscopic elastic materials have hysteretic nonlinear behaviors yielding acoustic and ultrasonic wave distortion, which gives rise to changes in the resonance frequencies as the amplitude of the excitation changes, generation of accompanying harmonics, nonlinear attenuation and multiplication of waves at different frequencies [15,16]. It has also been shown that cracks and delamination with low-aspect-ratio geometry are the scattering sources creating nonlinear waves, which arise from hysteresis in the wave pressure–deformation relation [17]. Wave scattering can be also caused by either horizontal or vertical mode conversion in which the energy of the incident Lamb waves at a specified driving frequency is redistributed into neighboring Lamb wave modes as illustrated in Fig. 2. Because delamination changes the internal geometric boundary conditions in a composite plate, diffraction and reflection of the waves can also produce wave scattering when the incident Lamb waves pass through delamination.

Because the TR of waves is fundamentally based on the linear reciprocity of the system [10,11], the linear reciprocity and the TR break down if there exists any source of nonlinearity along the wave path. Therefore, by comparing the discrepancy between the original input signal and the reconstructed signal, damage such as crack opening-and-closing, delamination and fiber breakage could be detected.

In most conventional damage detection techniques, damage is inferred by comparing newly obtained data sets with baseline data from measurements when the condition of the system was good. Because there might have been numerous variations since the baseline data were collected, it would be difficult to blame structural

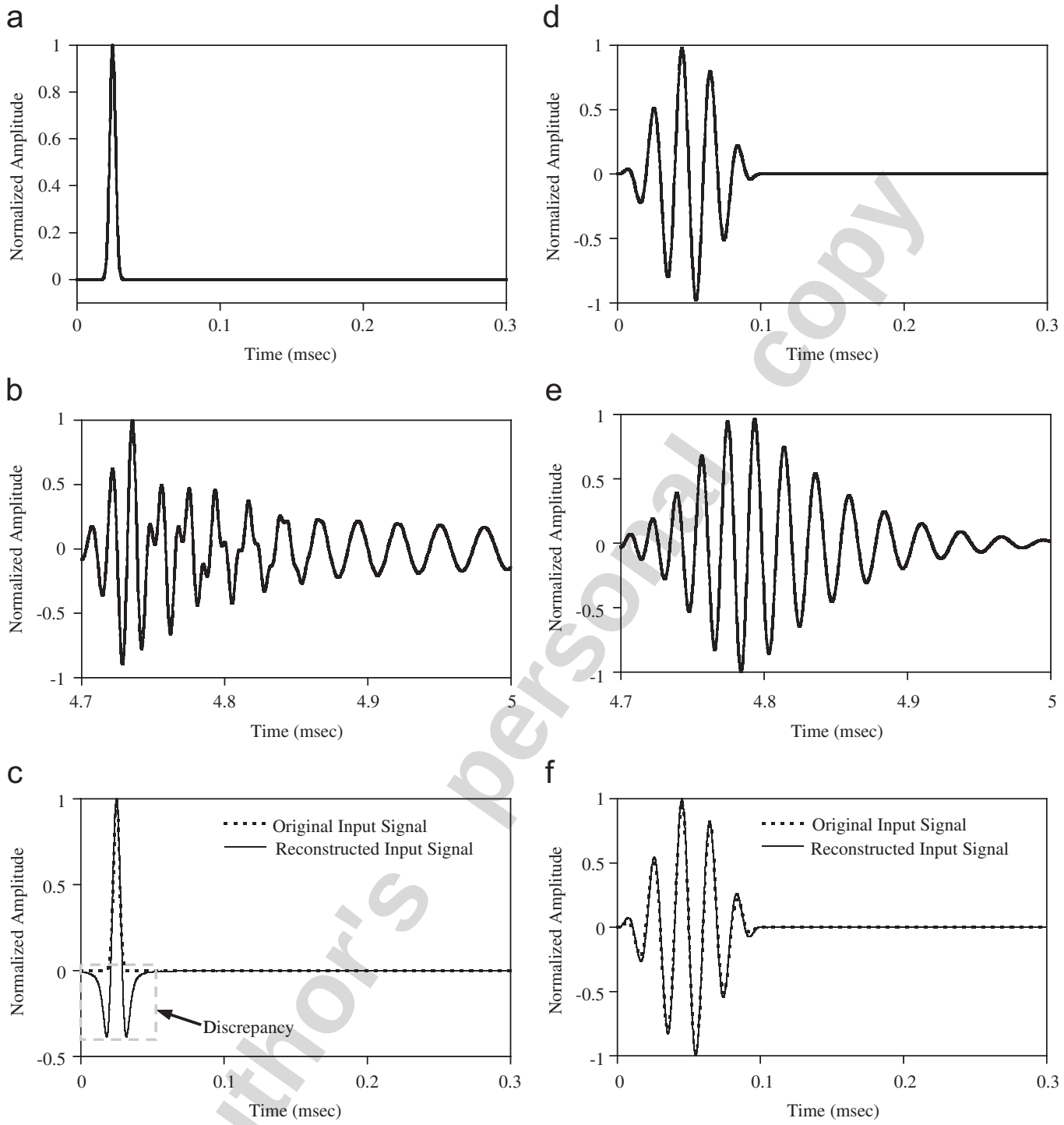

Fig. 5. Reconstruction of input signals using broad-band and narrowband input signals through a numerically simulated time reversal process. (a) Original input signal, a Gaussian pulse. (b) Response to a Gaussian pulse. (c) Original input (dotted) and reconstructed input (solid) signal for a Gaussian pulse. (d) Original input signal, a 100 kHz tone burst. (e) Response to a 100 kHz tone burst. (f) Original input (dotted) and reconstructed input (solid) signal for a 100 kHz tone burst.

damage for all changes in the measured signals. For instance, operational and environmental conditions may affect the system behavior and these conditions may be different from those present when the baseline data were collected. Therefore, data normalization, which attempts to distinguish signal changes originated from structural damage from those caused by natural variations of the system, needs to be addressed [18].

In this study, the dependency on the baseline data measured at some previous point in time is completely eliminated by almost instantly comparing the emitted input signal and the reconstructed input signal. Furthermore, the active PZT sensing system employed in this study allows for an easy implementation of the time reversal process. The generation of the input signal, excitation of the actuation PZT and acquisition of the response signal are fully automated and the entire time reversal process for one particular path takes less than a minute.

4. An enhanced time reversal method using wavelet signal processing

In the previous section, we have described the basic concept of time reversal analysis for Lamb wave propagation based on Mindlin plate theory. In this section, we discuss the use of wavelet-based signal processing techniques to enhance the TR of Lamb waves in the presence of background noise.

4.1. Active sensing using a known input waveform

First, a carefully designed narrowband input waveform is exerted onto a structure to minimize the frequency dependence of the time reversal operator and to maintain a high signal-to-noise ratio in the time reversal process. The advantage of using the narrowband input signal is to prevent the time reversal operator, $|G|^2$ in Eq. (1) from having large variations around the driving frequency. In addition, the use of a known and repeatable input further makes the subsequent signal processing for the time reversal process much easier and repeatable. A similar approach to noise elimination in ultrasonic signals used in flaw detection can be found in Ref. [19]. A Morlet wavelet function, as defined below, with a driving frequency of 110 kHz is adopted as an input waveform [20] and

$$\psi(t) = e^{-t^2/2}\cos(5t). \tag{13}$$

A proper selection of the driving frequency is critical for successful generation of Lamb waves in a given structure. Further discussion on the selection of the driving frequency can be found in Ref. [2].

4.2. Automated signal selection process based on wavelet transform

As discussed in Section 2, the time reversal analysis based on the Mindlin plate theory is limited only to the A_0 mode. When Lamb waves travel in a thin plate, a response signal, however, consists of several wave modes as illustrated in Fig. 6. Some of the modes are symmetric modes associated with the direct path of wave propagation and/or signals reflected off from the edges of the plate. There are also additional anti-symmetric modes reflected off from the edges. Because these reflected modes are very sensitive to the changes in boundary conditions, our primary interest lies in investigating the A_0 mode corresponding only to the direct path between the actuating PZT and the sensing PZT. Note that this A_0 mode traveling along the direct path between the actuator and the sensor is insensitive to changing boundary conditions. Therefore, only the A_0 mode portion of the signal needs to be extracted from the raw signal, and use this procedure to minimize false

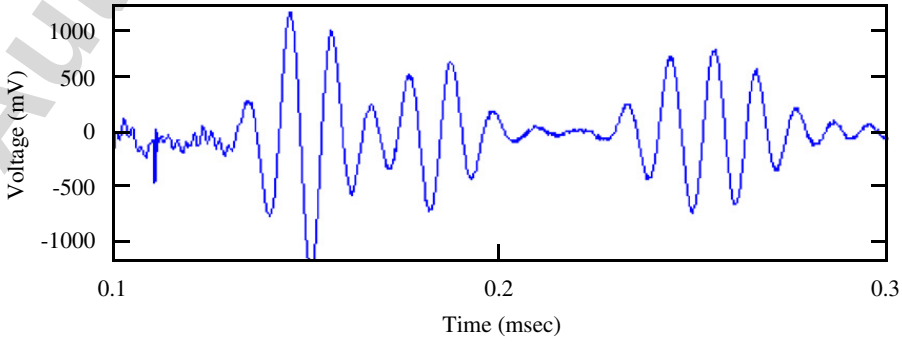

Fig. 6. A typical dynamic strain response measured at one of the piezoelectric sensors.

warnings of damage due to changing operational conditions of the system. Because this signal component of interest, the A_0 mode, is time and frequency limited, the two-dimensional time–frequency representation of the signal can be a useful tool for characterizing dispersive effects and analyzing multimodal signals. For this purpose, an automated selection procedure based on wavelet analysis is developed.

The basic concept of this automated selection procedure is as follows: if the signal shape that needs to be extracted for damage detection is known a priori, optimal extraction can be achieved by using a matched mother wavelet that models the shape of the signal component [21]. A schematic of the automated selection procedure is shown in Fig. 7. First, the continuous wavelet transform of the signal, $Wf(u,s)$, is obtained by convolving the signal $f(t)$ with the translations (u) and dilations (s) of the mother wavelet:

$$Wf(u,s) = \int_{-\infty}^{\infty} f(t)\frac{1}{\sqrt{s}}\psi^*_{u,s}(t)\,\mathrm{d}t, \tag{14}$$

where

$$\psi^*_{u,s}(t) = \frac{1}{\sqrt{s}}\psi\left(\frac{t-u}{s}\right). \tag{15}$$

The Morlet wavelet, defined in Eq. (13), is used as a mother wavelet $\Psi(t)$ in the wavelet transform. Then a complete set of daughter wavelets $\psi^*_{u,s}(t)$ is generated from the mother wavelet by the dilation (s) and shift (u) operations. Note that each value of the wavelet coefficient $Wf(u,s)$ is normalized by the factor $1/\sqrt{s}$ to ensure that the integral energy given by each wavelet is independent of the dilation s.

Because the Morlet wavelet is used as a mother wavelet, the wavelet coefficient is the correlation between the signal and the mother wavelet, and the wavelet coefficient arrives at its maximum value when the shape of the response signal is closest to that of the Morlet wavelet. When this search for the maximum wavelet coefficient is performed at the input frequency, the time portion of the A_0 mode can be easily detected by the temporal

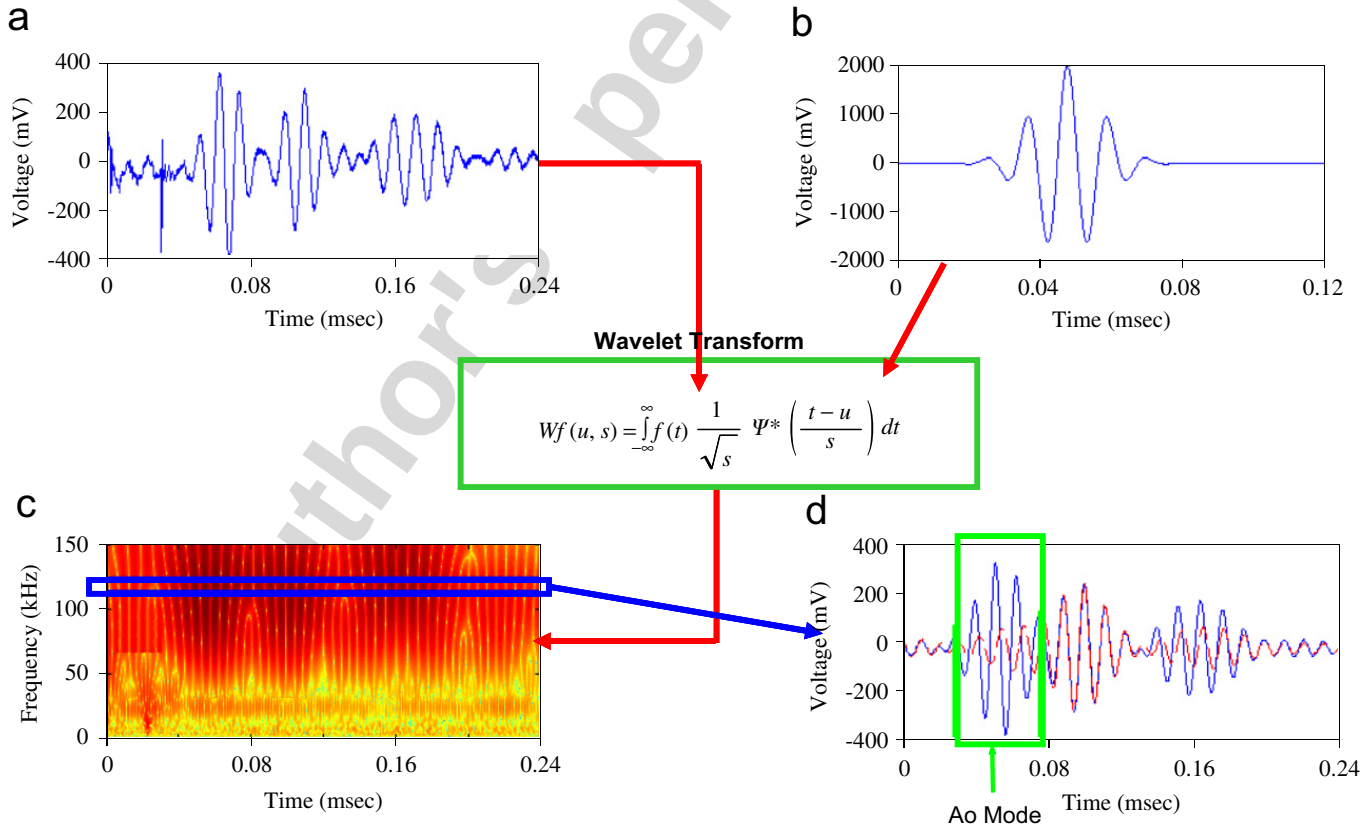

Fig. 7. A wavelet analysis procedure for automated signal selection: (a) response time signal, (b) input Morlet wavelet at 110 kHz, (c) time–frequency response and (d) time response at input frequency.

shift parameter u. Hence, this wavelet transform can be an effective way to reduce noise if the mother wavelet is chosen to be a good representation of the signal to be detected. Furthermore, the continuous wavelet transform is performed instead of the discrete wavelet transform to obtain better time resolution over the full period of the signal [22]. Through this automated selection procedure, only the A_0 mode of the response time signal is chosen for reemission. This selection procedure also automatically eliminates the portion of the response signal contaminated by electromagnetic interference.

4.3. Signal filtering based on multiresolution analysis

As described previously, the driving frequency of the narrowband excitation can be selected so that only two fundamental modes are generated for wave propagation. Then, different wave speeds of these two modes are compensated for during the time reversal process when they are reversed in time before being remitted. However, the frequency content of the traveling waves smears into nearby frequencies and is non-uniformly amplified during the time reversal process. Therefore, to enhance the TR of the reconstructed signal at the original input point, the measured response signal needs to be processed before reemitting at the response point. In particular, for the time reversal analysis of Lamb waves, it is critical to retain the response components only at the original input frequency value, because of the frequency-dependent nature of the time reversal operator shown in Fig. 4. To achieve this goal, a multiresolution analysis is adopted to filter out the measurement noise in the response signals and to keep only the response component at the driving frequency value. Multiresolution signal processing based on wavelet transform has been extensively studied especially for perfect reconstruction of signals by using quadrature mirror filters [23].

Once the wavelet coefficients are computed from Eq. (14), the original signal can be reconstructed via the following inverse continuous wavelet transform [23]:

$$f(t) = \frac{1}{C_\varphi} \int_{-\infty}^{\infty} \int_{-\infty}^{\infty} Wf(u,s) \frac{1}{\sqrt{s}} \psi\left(\frac{t-u}{s}\right) \frac{1}{s^2} \, \mathrm{d}s \, \mathrm{d}u, \tag{16}$$

where C_φ is a constant determined by

$$C_\psi = \int_0^{\infty} \frac{|\psi|}{\omega} \, \mathrm{d}\omega. \tag{17}$$

In this study, the integration operation with respect to the scale parameter s in Eq. (16) is restricted to include only that part near the driving frequency in order to filter out frequency components outside the driving frequency before transmitting the response signal back to the original input location, thus:

$$f(t) = \frac{1}{C_\varphi} \int_{-\infty}^{\infty} \int_{a}^{b} Wf(u,s) \frac{1}{\sqrt{s}} \psi\left(\frac{t-u}{s}\right) \frac{1}{s^2} \, \mathrm{d}s \, \mathrm{d}u, \tag{18}$$

where a and b are the lower and upper limits of the narrowband excitation frequency. The choice of the frequency limits is dictated by the fact that the filter must cover the frequency range of interest so that useful information is not lost. In fact, the wavelet transform is used as a matched filter to improve the signal-to-noise ratio without any loss in time resolution or accuracy and in many cases with improvements. This filtering processing is repeated for the reconstructed input signal obtained by the time reversal process. An example of the result of using this filtering process is shown in Fig. 8. This filtering process tends to minimize the measurement noise in the response signal and keep the response component only at the driving frequency. It is observed that this filtering process improves the TR of Lamb waves.

5. Experimental study

The overall test configuration of this study is shown in Fig. 9(a). The test setup consists of a composite plate with a surface-mounted sensor layer, a personal computer with a built-in data acquisition system and an external signal amplifier. The dimension of the composite plates is 60.96 cm × 60.96 cm × 0.6350 cm (24 in × 24 in × 1/4 in). The quasi-isotropic plate contains 48 plies stacked according to the sequence [6(0/45/–45/90)]s, consisting of Toray T300 Graphite fibers and a 934 Epoxy matrix.

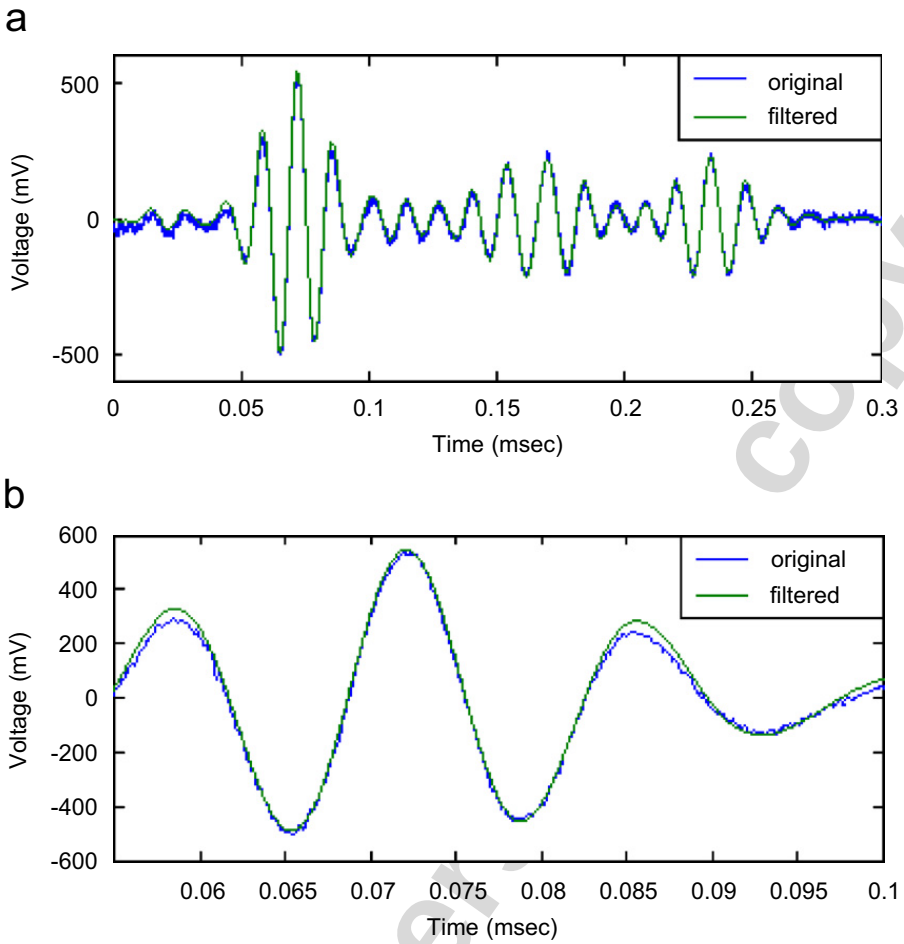

Fig. 8. The raw signal (solid) and the restored signal (dotted) after filtering: (a) before zooming and (b) after zooming.

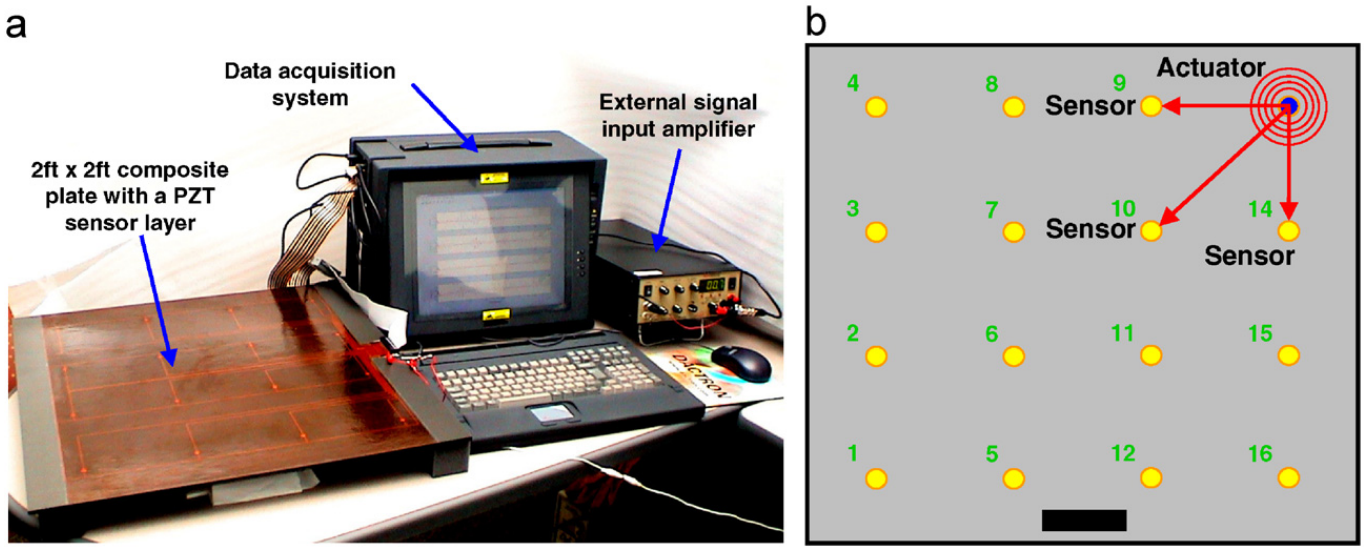

Fig. 9. An active sensing system for detecting delamination on a composite plate: (a) testing configuration and (b) the layout of the PZT sensors/actuators.

A commercially available thin film with embedded PZT sensors is mounted on one surface of the composite plate as shown in Fig. 9(b) [24]. A total of 16 PZT patches are used as both sensors and actuators to form an "active" local sensing system. Because the PZTs produce an electrical charge when deformed, the PZT patches

can be used as dynamic strain gauges. Conversely, the same PZT patches can also be used as actuators, because elastic waves are produced when an electrical field is applied to the patches. These PZT sensor/actuators are inexpensive, generally require low power and are relatively non-intrusive.

The personal computer shown in Fig. 9(a) has built-in analog-to-digital and digital-to-analog converters, controlling the input signals to the PZTs and recording the measured response signals. Increasing the amplitude of the input signal yields a clearer signal, enhancing the signal-to-noise ratio. On the other hand, the input voltage should be minimized for field applications, requiring as low power as possible. In this experiment, the optimal input voltage was designed to be near 45 V, producing 1–5 V output voltage at the sensing PZTs. For the time reversal analysis, a tone burst excitation is created at 110 kHz so that only two fundamental modes are generated as shown in Fig. 2 and the magnitude of the time reversal operator shown in Fig. 4 is maximized. PZTs in a circular shape are used with a diameter of only 0.64 cm (1/4 in). The wave velocity at the driving frequency of 110 kHz is around 3500 m/s and gives a wavelength of 31.8 mm, which is much bigger than the size of PZT. The sensing spacing is set to 15.24 cm (6 in). A discussion on the selection of design parameters such as the dimensions of the PZT patches, sensor spacing and a driving frequency can be found in Ref. [25].

The strain responses measured from the experimental study and simulated by the Mindlin plate theory are shown in Fig. 10 for a wave propagation path corresponding to the actuating PZT #15 and the sensing PZT #16. The measured strain response corresponding to the first flexural A_0 mode is well-predicted by the Mindlin plate theory as shown in Fig. 10. It should be noted that because the Mindlin plate theory, which approximates the Rayleigh–Lamb equations for an infinite plate, is used to predict only the wave propagation of the A_0 mode corresponding to the direct path between the actuating and sensing PZTs, the additional wave modes reflected off from the boundaries of the plate are not predicted by the Mindlin plate theory. The simulated strain response is obtained from Eqs. (4) and (5). The elasticity modulus and Poisson ratio are approximated by assuming a quasi-isotropic composite plate [2]. It should be noted that the approximated elasticity modulus and Poisson ratio are properly calibrated so that the arrival time of the simulated and measured waves coincides. Without calibration, it is observed that the simulated wave travels slightly slower than the measured wave while the shapes of the simulated and the measured waves are almost identical.

Typical results of the enhanced time reversal method obtained from the composite plate used in this study are shown in Fig. 11. First, one PZT patch is designated as an actuator, exerting a predefined waveform into the structure (Fig. 11(a)). Then, an adjacent PZT becomes a strain sensor and measures a response signal (Fig. 11(b)). Once the traveled waves are measured at the response point, the measured signal is processed by using the wavelet-based signal processing procedures described in Section 4. First, the A_0 segment of the response signal is selected via the proposed autonomous selection scheme. Then, the wavelet-based filtering is applied to the response signal to retain only the response component at the driving frequency. In Fig. 11(c) is shown the A_0 mode selected from the response signal shown in Fig. 11(b) after being filtered and reversed in time. This processed response signal is reemitted from the previous sensing PZT, which is now an actuator. The reconstructed response signal at the original input PZT location is shown in Fig. 11(d). This process of the

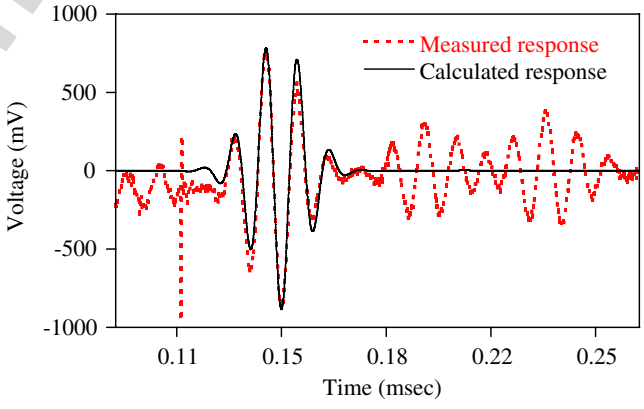

Fig. 10. The calculated (solid) and the measured (dotted) strain response of the path from PZT#15 to PZT#16.

Lamb wave propagation and the time reversal analysis are repeated for different combinations of actuator–sensor pairs. A total of 66 different path combinations are investigated. Finally, the original input signal and the reconstructed signal at the original input point are shown for the actuation PZT #1 and the sensing PZT #6 in Fig. 12.

Our ultimate goal is to estimate damage by comparing the shape of the original input signal with that of the reconstructed signal. Results in Fig. 12 demonstrate that the initial input waveform is well restored through the enhanced time reversal method when there is no defect in the composite plate tested. A TR index based on this observation is defined as follows:

$$\mathrm{TR} = 1 - \sqrt{\left\{\int_{t_0}^{t_1} I(t)V(t)\,\mathrm{d}t\right\}^2 \Big/ \left\{\int_{t_0}^{t_1} I(t)^2\,\mathrm{d}t \int_{t_0}^{t_1} V(t)^2\,\mathrm{d}t\right\}}, \tag{19}$$

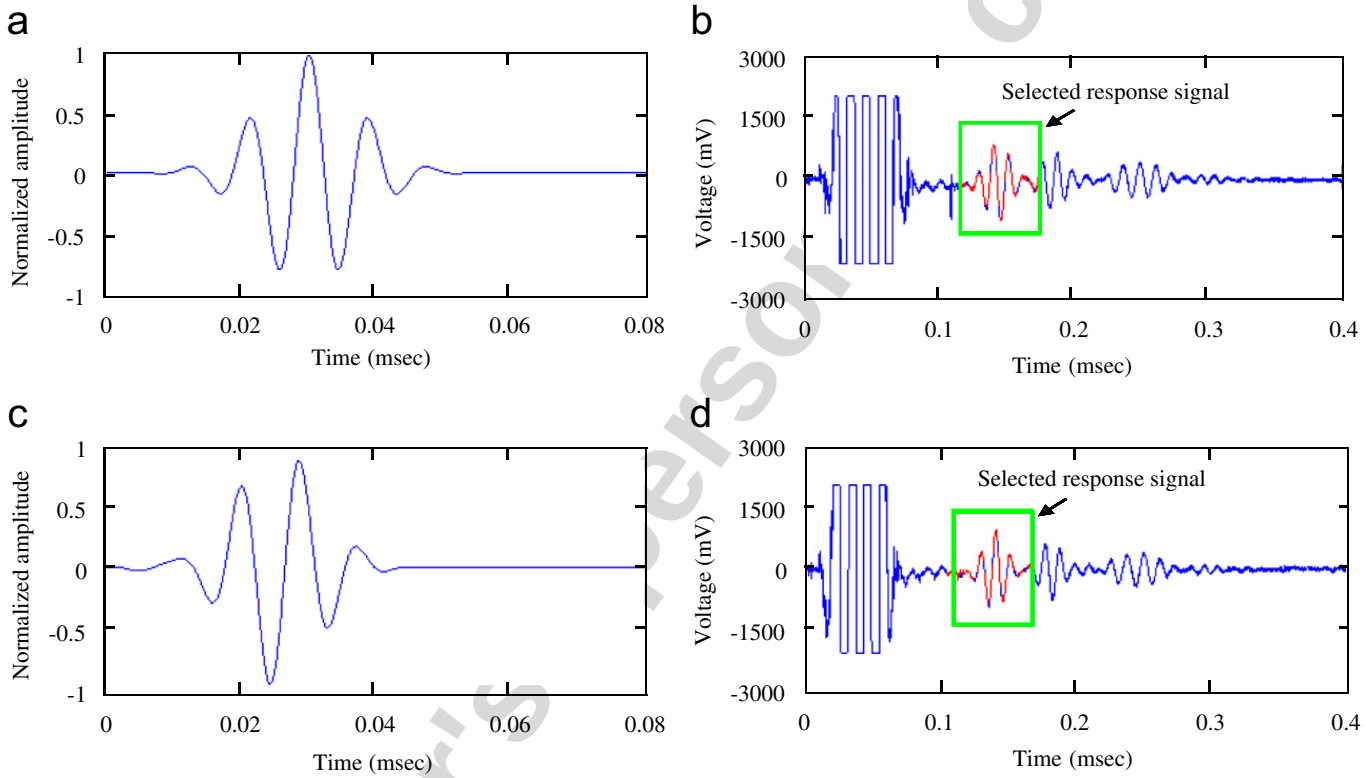

Fig. 11. Measured time signals at various stages of the time reversal analysis: (a) an original input Morlet waveform, (b) a response signal at a sensing PZT, (c) a time-reversed response signal after signal processing and (d) a response signal at the original actuating PZT.

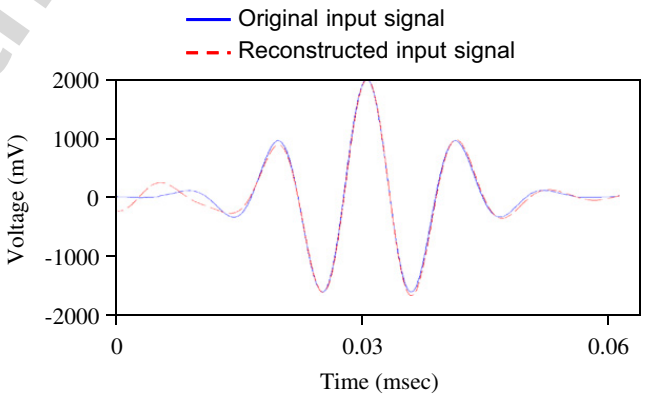

Fig. 12. The original input signal (solid) and the restored signal (dotted) after the automated selection and filtering.

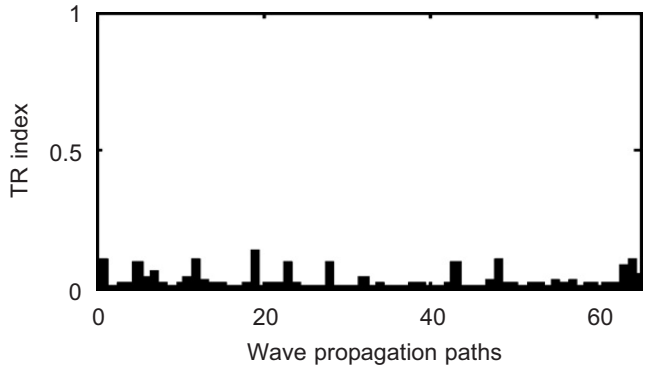

Fig. 13. Time reversibility (TR) index computed for 66 different wave propagation paths.

where the $I(t)$ and $V(t)$ denote the known input and reconstructed signals. t_0 and t_1 represent the starting and ending time points of the baseline signal's first A_0 mode. The value of DI becomes zero when the TR of Lamb waves is preserved. Note that the root square term in Eq. (19) becomes 1.0 if and only if $V(t) = \beta I(t)$ for all t where $t_0 \leqslant t \leqslant t_1$ and β is a non-zero constant. Therefore, simple linear attenuation of a signal will not alter the damage index value. If the reconstructed signal deviates from the input signal, the damage index value increases and approaches 1.0, indicating the existence of damage along the direct wave path.

In Fig. 13, the computed TR index values are shown for all 66 paths. For most cases, the TR index values stay below 0.1. The mean and standard deviation of the 66 TR values are 0.027 and 0.034, respectively. Subsequent destructive testing of the composite plate reported in Ref. [26] reveals that this TR value increases significantly once damage is introduced along the wave propagation path. Once the TR index value exceeds a pre-specified threshold value, the corresponding signal is defined as damaged.

One potential advantage of the time reversal analysis is that damage might be inspected without requiring any baseline data to be obtained at some previous time. This advantage over conventional damage detection techniques helps minimize false warnings of damage. For instance, if the operational temperature or boundary conditions of a system change after the baseline data are collected, most pattern recognition techniques will have difficulties in discerning signal changes caused by damage from those due to the temperature or boundary condition changes. In other words, if there are any changes in the newly measured signal since the baseline signal is obtained, it is hard to determine what is causing this change. However, by instantly comparing the input waveform with the reconstructed signal, the time-dependent issue of the conventional pattern recognition techniques can be eliminated, making it much easier to distinguish signal changes caused by damage from those caused by natural variation of the system.

6. Summary and discussion

In this study, the applicability of a time reversal method to health monitoring of a composite plate is investigated. In particular, a unique input waveform and signal processing techniques are employed to improve the TR of Lamb waves. First, a narrowband excitation waveform is employed to address the frequency dependence of the time reversal operator. Then, an automated signal selection process is developed based on a wavelet transform to retain only a segment of a raw response signal that is more sensitive to damage and less responsive to changing boundary conditions. In addition, wavelet-based filtering is performed to enhance the TR further by taking advantage of temporal and spectral differences between the signal component of our interest and background noise. By using an active sensing system mounted on a composite plate, it has been demonstrated that an input waveform exerted at an actuating PZT can be reconstructed at the excitation point after processing the response signal measured at a distance from the excitation point and reemitting the processed signal at the sensing location after being reversed in time. The reconstructed signal will deviate from the known input signal if there are certain types of defects along the wave propagation paths. Further research is underway to investigate the effects of different types of defects on the TR.

The development of a technique is currently underway to classify different representative damage types based on the distortion characteristics between the input waveform and the reconstructed signal. Further research is also warranted to optimally design the parameters of the active sensing system, such as the spacing between the PZT patches, the actuating frequency and the power requirement for the PZTs. It should be pointed out that the procedure developed in this study has only been verified on a relatively simple laboratory test specimen. To fully verify the proposed approach, it will be necessary to apply the proposed approach to different types of representative structures.

Acknowledgments

This research is partially sponsored by Los Alamos National Laboratory, Contract Number 75067-001-03. Funding for this project has been provided by the Department of Energy through the internal funding program at Los Alamos National Laboratory known as Laboratory Directed Research and Development (Damage Prognosis Solutions). Additional support has been provided from the National Science Foundation, Grant number CMS-9988909. The first author would like to acknowledge the Post-Doctoral Fellowship Program of Korea Science & Engineering Foundation (KOSEF), which provides support for his stay at Stanford University.

References

[1] E. Moulin, J. Assaad, C. Delebarre H. Kaczmarek, D. Balageas, Piezoelectric transducer embedded in a composite plate: application to Lamb wave generation, *Journal of Applied Physics* 82 (5) (1997) 2049–2055.
[2] H. Sohn, G. Park, J.R. Wait., N.P. Limback, C.R. Farrar, Wavelet-based active sensing for delamination detection in composite structures, *Smart Materials and Structures* 13 (1) (2004) 153–160.
[3] C.A. Paget, S. Grondel, K. Levin, C. Delebarre, Damage assessment in composites by Lamb waves and wavelet coefficients, *Smart Materials and Structures* 12 (3) (2003) 393–402.
[4] S.S. Kessler, C.E. Johnson, C.T. Dunn, Experimental application of optimized Lamb wave actuating/sensing patches for health monitoring of composite structures, *Proceedings of the Fourth International Workshop on Structural Health Monitoring*, Stanford University, 2003, pp. 429–436.
[5] C.H. Wang, J.T. Rose, F.K. Chang, A computerized time-reversal method for structural health monitoring. *Proceedings of SPIE Conference on Smart Structures and NDE*, San Diego, CA, USA, 2003.
[6] C. Prada, M. Fink, Separation of interfering acoustic scattered signals using the invariants of the time-reversal operator. Application to Lamb waves characterization, *Journal of the Acoustical Society of America* 104 (2) (1998) 801–807.
[7] R.K. Ing, M. Fink, Time recompression of dispersive Lamb waves using a time reversal mirror—application to flaw detection in thin plates, *IEEE Ultrasonics Symposium* 1 (1996) 659–663.
[8] R.K. Ing, M. Fink, Time-reversed Lamb waves, *IEEE Transactions on Ultrasonics, Ferroelectrics, and Frequency Control* 45 (4) (1998) 1032–1043.
[9] M. Fink, Time-reversed acoustics, *Scientific American* 281 (5) (1999) 91–97.
[10] C. Draeger, D. Cassereau, M. Fink, Theory of the time-reversal process in solids, *Journal of the Acoustical Society of America* 102 (3) (1997) 1289–1295.
[11] M. Fink, C. Prada, Acoustic time-reversal mirrors, *Inverse Problems* 17 (2001) R1–R38.
[12] D.N. Alleyne, T.P. Pialucha, P. Cawley, A signal regeneration technique for long-range propagation of dispersive Lamb waves, *Ultrasonics* 31 (3) (1993) 201–204.
[13] I.A. Viktorov, *Rayleigh and Lamb Waves*, Plenum Press, New York, 1967.
[14] L.R.F. Rose, C.H. Wang, Mindlin plate theory for damage detection, source solutions, *The Journal of the Acoustical Society of America* 116 (1) (2004) 154–171.
[15] R.A. Guyer, P.A. Johnson, Nonlinear mesoscopic elasticity: evidence for a new class of materials, *Physics Today* April (1999) 30–36.
[16] K.V.D. Abeele, P.A. Johnson, A. Sutin, Nonlinear elastic wave spectroscopy (NEWS) techniques to discern material damage, part I: nonlinear wave modulation spectroscopy (NWMS), *Research in Nondestructive Evaluation* 12 (2000) 17–30.
[17] V.V. Kazakov, A. Sutin, P.A. Johnson, Sensitive imaging of an elastic nonlinear wave-scattering source in a solid, *Applied Physics Letters* 81 (4) (2002) 646–648.
[18] H. Sohn, Effects of environmental and operational variability on structural health monitoring, *A Special Issue of Philosophical Transaction of Royal Society A on Structural Health Monitoring* 365 (2007) 539–560.
[19] A. Abbate, J. Koay, J. Frankel, S.C. Schroeder, P. Das, Signal detection and noise suppression using a wavelet transform signal processor: application to ultrasonic flaw detection, *IEEE Transactions on Ultrasonics, Ferroelectrics, and Frequency Control* 44 (1) (1997) 14–26.
[20] G. Strang, T. Nguyen, *Wavelets and Filter Banks*, Wellesley-Cambridge Press, Wellesley, MA, 1997.

[21] P. Das, *Optical Signal Processing: Fundamental*, Springer, New York, NY, 1991.
[22] C.S. Burrus, R.A. Gopinath, H. Guo, *Introduction to Wavelets and Wavelet Transforms*, Prentice Hall, Upper Saddle River, NJ, 1998.
[23] A.N. Akansu, R.A. Haddad, *Multiresolution Signal Decomposition*, Academic Press, San Diego, CA, 1992.
[24] http://www.acellent.com.
[25] S.S. Kessler, Piezoelectric-based in-situ damage detection of composite materials for structural health monitoring systems, PhD Thesis, MIT Press, Cambridge, MA, 2002.
[26] H. Sohn, H.W. Park, K.H. Law, C.R. Farrar, Damage detection in composite plates by using an enhanced time reversal method, *ASCE, Journal of Aerospace Engineering*, 2007, accepted.